Journal of Controlled Release 385 (2025) 113939

Contents lists available at ScienceDirect

Journal of Controlled Release

journal homepage: www.elsevier.com/locate/jconrel

Intravitreal injection of cell membrane-coated nanoparticles for retinoblastoma treatment

Yichi Zhang [a,b,c], Kaiqi Long [a,b,c], Ka Yi Lee [a,c], Jia Li [a,b,c], Shuting Xu [a,b,c], Kang Chen [a,c], Xi Chen [a,b,c], Qingyi Dai [a,c,d], Yifan Lin [d], Changyou Zhan [e], Weiping Wang [a,b,c,*]

[a] State Key Laboratory of Pharmaceutical Biotechnology, The University of Hong Kong, Hong Kong SAR, China
[b] Department of Pharmacology & Pharmacy, Li Ka Shing Faculty of Medicine, The University of Hong Kong, Hong Kong SAR, China
[c] Laboratory of Molecular Engineering and Nanomedicine, Dr. Li Dak-Sum Research Centre, The University of Hong Kong, Hong Kong SAR, China
[d] Division of Paediatric Dentistry and Orthodontics, Faculty of Dentistry, The University of Hong Kong, Hong Kong SAR, China
[e] Department of Pharmacology, School of Basic Medical Sciences & State Key Laboratory of Molecular Engineering of Polymers, Fudan University, Shanghai 200032, China

ARTICLE INFO

Keywords:
Intravitreal injection
Intraocular drug delivery
Retinoblastoma
Cell membrane-coated nanoparticles
Homotyic targeting

ABSTRACT

Chemotherapy is a widely adopted treatment for malignant intraocular tumors such as retinoblastoma. However, achieving high delivery efficiency remains challenging due to rapid clearance and lack of targeting specificity. Cancer cell membrane-coated nanoparticles have been extensively reported to exhibit specific affinity to homotypic cancer cells. Here we designed poly (lactic-co-glycolic acid) (PLGA)-based polymeric nanoparticles coated with the plasma membrane of WERI-Rb-1 cells, derived from human retinoblastoma. These nanoparticles showed remarkable affinity to WERI-Rb-1 cells in vitro. Loaded with the FDA-approved chemotherapy drug etoposide, the nanoparticles exhibited excellent antitumor efficacy and excellent biosafety following a single-dose intravitreal injection in vivo. Overall, this work presents a simple yet effective strategy for the treatment of retinoblastoma.

1. Introduction

Retinoblastoma is a type of malignant intraocular cancer that originates from retina area [1]. Commonly diagnosed in infancy and childhood, its mortality reaches to 70 % in countries of middle and low income [2]. Enucleation and systemic chemotherapy are common strategies for medical management of retinoblastoma. Enucleation can prevent potential spread of the tumor cells efficiently. However, removal of eyes will lead to blindness, especially for patients with tumors on both sides [3]. Systemic chemotherapy provides a conservative treatment method for retinoblastoma, but its unwanted toxicity on off-target tissues and low delivery efficiency are unavoidable problems [4]. In comparison, local chemotherapy such as intravitreal drug injection could waive the systemic toxicity. However, free drug intravitreally injected was prone to quick leakage and clearance [5]. Drug-loaded nanoparticles can be an alternative to overcome the drawbacks of free drug administration by increasing solubility and sustaining drug release [6]. Moreover, rational design and modification of nanoparticles could endow the nanoparticles with tumor targeting ability to further improve the drug delivery efficiency [7].

Biomimetic camouflage has been an effective strategy for nanoparticles functionalization [8]. For instance, owing to the reservation of functional proteins on surface of the plasma membrane, cell membrane-coated nanoparticles using common cells such as red blood cells and macrophages have been reported for the treatment of intraocular diseases such as choroidal neovascularization (CNV) and retinoblastoma [9–11]. Moreover, cancer cell membrane-coated nanoparticles have been verified to have specific affinity toward homotypic cancer cells, which is called as homotypic targeting effect [12]. Along this line, many types of cancer cell membrane-coated nanoparticles have been developed for the treatment of homotypic cancer. For example, doxorubicin-loaded PLGA nanoparticles coated with cell membrane derived from HepG2 cells showed excellent antitumor efficacy against hepatocellular carcinoma [13]. Similar strategies have also been applied for the

* Corresponding author at: State Key Laboratory of Pharmaceutical Biotechnology, The University of Hong Kong, Hong Kong SAR, China.
E-mail address: wangwp@hku.hk (W. Wang).

https://doi.org/10.1016/j.jconrel.2025.113939
Received 3 February 2025; Received in revised form 4 June 2025; Accepted 5 June 2025
Available online 6 June 2025
0168-3659/© 2025 The Authors. Published by Elsevier B.V. This is an open access article under the CC BY license (http://creativecommons.org/licenses/by/4.0/).

treatment of head and neck squamous cell carcinoma and mammary carcinoma [14–16]. However, cancer cell membrane-coated nanoparticles have not been applied for the treatment of intraocular tumors yet.

In this study, we designed a human retinoblastoma cell membrane-coated nanoplatform. WERI-Rb-1, a continuous cell line derived from human retinoblastoma and commonly used in preclinical research, was selected as the cell membrane source [17]. Besides the reported homotypic targeting effect of cancer cell membrane-coated nanoparticles, we observed a tendency for WERI-Rb-1 cells to aggregate in cell culture. Based on these, we hypothesized that nanoparticles coated with WERI-Rb-1 cell membrane would have significant targeting effect to human retinoblastoma (Scheme 1). Biocompatible and biodegradable copolymer PLGA was chosen as the building block of the nanoparticle core. A typical FDA-approved antitumor chemotherapy drug, etoposide, which is a DNA topoisomerase II inhibitor, was selected as therapeutic agent loaded in the PLGA nanoparticles [18]. The homotypic targeting effect and enhanced cytotoxicity of the coated nanoparticles were demonstrated in vitro. By a single-dose intravitreal injection, the antitumor efficacy was then verified in vivo in an orthotopic human retinoblastoma-bearing mouse model.

2. Materials and methods

2.1. Materials

PLGA (50:50, ester-terminated, M.W. = 45,000), chlorpromazine (CPZ), genistein and m-β-cyclodextrin (mβ-CD) were all obtained from Sigma-Aldrich (MA, USA). $mPEG_{5000}$-$PLGA_{5000}$ (For PLGA part, 50:50, ester-terminated) was obtained from Yuanye (Shanghai, China). cRGD-PEG_{2000}-$PLGA_{12000}$ was obtained from Ruixibio (Xi'an, China). Etoposide was obtained from Bidepharm (Shanghai, China). Tris-HCl buffer, Versene solution (0.02 % EDTA DPBS solution), membrane and cytosol protein extraction kit, and Annexin V-FITC apoptosis detection kit were obtained from Beyotime (Shanghai, China). DiD dye, DiR dye, and D-luciferin potassium salt were obtained from Aladdin (Shanghai, China). Phenylmethanesulfonylfluoride (PMSF), Hoechst blue 33342, and DAPI were obtained from Thermo Fisher Scientific (MA, USA). EIPA and CCK-8 kit were obtained from MedChemExpress (MCE, Shanghai, China). Dichloromethane, acetonitrile, and acetone were obtained from Anaqua (DE, USA).

2.2. Cell culture

WERI-Rb1 human retinoblastoma cells (HTB-169, American Type Culture Collection) and transfected WERI-Rb1-GFP-Luc cells were cultured at 37 °C in 5 % CO_2 with Roswell Park Memorial Institute (RPMI) 1640 medium (Gibco) supplemented with 10 % fetal bovine serum (FBS; Gibco) and 1 % penicillin- streptomycin (Pen-Strep; Gibco). 4T1 mouse breast cancer cells (CRL-2539, American Type Culture Collection) and KYSE450 human esophageal cancer cells (CVCL_1353; Cellosaurus) were cultured at 37 °C in 5 % CO_2 with Dulbecco's Modified Eagle's Medium (DMEM; Gibco) supplemented with 10 % FBS and 1 % Pen-Strep.

2.3. Cell membrane extraction

The cell membrane of WERI-Rb1 cells was extracted with a commercially available membrane and cytosol protein extraction kit (Beyotime) under the guidance of the protocol. PMSF (1 mM) was supplemented in the extraction buffer for protease inhibition. A freeze-thaw cycling process was adopted for cell lysis. The collected cell membrane was stored in Versene solution. Weight of the extracted cell membrane was quantified after lyophilization.

2.4. Preparation of cell membrane-coated nanoparticles

A reported single emulsion method was adopted for the preparation of PLGA-etoposide nanoparticles (PE NPs) [19]. In details, 250 μL 50 mg/mL PLGA in dichloromethane and 250 μL 10 mg/mL etoposide in acetone were mixed and added to 2.5 mL 10 mM tris-HCl (pH = 8). The mixture was then sonicated for 2 min (100 W, 2 s on/1 s off, Sonics

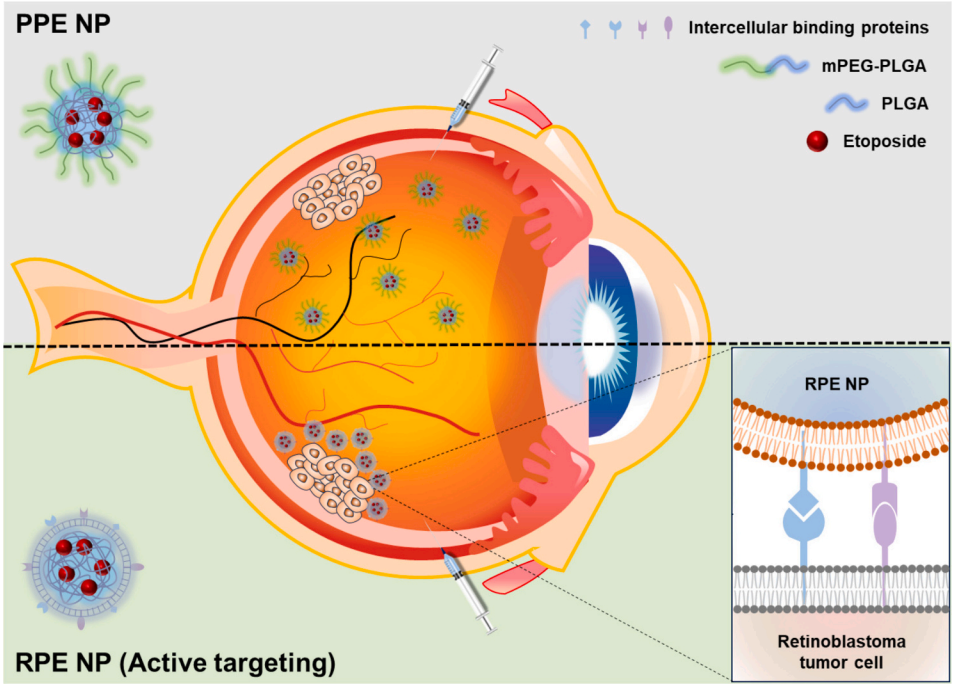

Scheme 1. Graphic scheme of WERI-Rb-1 cell membrane-coated nanoparticles (RPE NPs) for targeted drug delivery to retinoblastoma. Compared to PEGylated nanoparticles (PPE NPs), RPE NPs show a significant targeting effect toward retinoblastoma, attributed to the homotypic targeting effect facilitated by intercellular binding proteins on their surfaces.

VCX500 Ultrasonic Processors). For PLGA nanoparticles loaded with cell labelling dye DiD (ex/em = 644/663 nm) and DiR (ex/em = 748/780 nm), the preparation method was the same, and the dye solution was 5 μg/mL in 250 μL DCM. After the sonication, the mixture was added to 5 mL 10 mM tris-HCl (pH = 8) and stirred overnight at 800 rpm. The polymeric nanoparticles were collected as pellets after centrifugation at 23,000 *g* for 10 min. The PLGA-based nanoparticles were mixed with cell membrane suspension and sonicated in an Elmasonic EASY 100H bath sonicator for 5 min. The membrane-coated nanoparticles were resuspended in deionized water.

2.5. Drug encapsulation and loading of PE NPs

Drug encapsulation efficiency and loading capacity were measured by high performance liquid chromatography (Agilent 1260 Infinity II). RPE NP samples were dissolved in 50 % acetonitrile. The solution was eluted through the column at a flow rate of 1.5 mL/min and the etoposide was detected at a wavelength of 254 nm (Table S1). Encapsulation efficiency and loading capacity were calculated according to the following formulas:

$$\text{Encapsulation efficiency}\ (\%) = \frac{\text{Weight of loaded etoposide}}{\text{Weight of fed etoposide}} \times 100\%$$

$$\text{Loading capacity}\ (\%) = \frac{\text{Weight of loaded etoposide}}{\text{Weight of PE NPs}} \times 100\%$$

2.6. Physical characterization of the nanoparticles

Size distribution and zeta potential of the nanoparticles were measured by using a dynamic light scattering (DLS) machine (Zetasizer Nano ZS90, Malvern). The morphology of the nanoparticles and cell membrane vesicles was visualized by using a transmission electron microscope (CM100, Philips). The presence of plasma membrane proteins was verified by sodium dodecyl sulfate–polyacrylamide gel electrophoresis (SDS-PAGE). The UV–Vis spectra of the nanoparticles and free etoposide were characterized by a microplate reader (SpectraMax M4).

2.7. Optimization of RPE NPs formulation

WERI-Rb-1 cell membrane was mixed with PE NPs in deionized water. With fixed total volume and fixed PE NPs weight concentration (1 mg/mL), the WERI-Rb-1 cell membrane's weight concentration was set to be 0.25, 0.5, 1, 2, and 4 mg/mL. After coating through ultrasound water bath, the average sizes of the coated nanoparticles at different membrane/core weight ratios were measured. The solvent of the coated nanoparticles solutions was transferred to be PBS buffer (1×) by adding an equal volume of PBS buffer (2×). The average sizes of the nanoparticles were then measured. After 14 days at room temperature, the average sizes of the nanoparticles were measured again to evaluate the stability of the coated nanoparticles at different membrane/core weight ratios.

2.8. Drug release profile of RPE NPs

RPE NP solution (1 mg/mL, 140 μL) was added into Slide-A-Lyzer MINI dialysis devices (10 K molecular weight cutoff; Thermo Fisher Scientific) and floated on 14 mL PBS buffer under shaking at 60 rpm and 37 °C. The RPE NP solution was retrieved at different timepoints and centrifugated at 23,000 *g* for 10 min for collection. The pellets were dissolved in 50 % acetonitrile for HPLC analysis to quantify the remaining etoposide content.

2.9. In vitro homotypic targeting effect of RPDiD NPs

In vitro targeting property of RPDiD NPs was verified by evaluation of cellular uptake. The DiD dye concentration was quantified by a microplate reader (SpectraMax M4, Fig. S1b). WERI-Rb1 cells were seeded in a 12-well plate at density of 10^5 cells per mL per well and incubated for 24 h. The cells were divided into 4 groups according to different treatments: PBS, PPDiD NPs, cRGD-PPDiD NPs and RPDiD NPs. After 0.5 h treatment, the cells were washed by PBS three times for flow cytometry analysis. For confocal imaging, after the treatment, the cells were stained with DAPI for 10 min and washed by PBS three times. The cells were mounted on slides for confocal imaging (Zeiss LSM 880). For homotypic property verification, WERI-Rb1 cells, HeLa cells, and KYSE450 cells were seeded in a 12-well plate at a density of 10^5 cells per mL per well. After 24 h incubation, all the cells were treated with RPDiD NPs for 0.5 h. The cells were collected and washed by PBS three times for flow cytometry analysis.

2.10. Mechanism of RPE NPs uptake by WERI-Rb-1 cells

WERI-Rb-1 cells were seeded in a 24-well plate at density of 5×10^4 cells per mL per well. The cells were pretreated with chlorpromazine (5 μg/mL), genistein (25 μg/mL), mβ-CD (5 μg/mL), or EIPA (20 μM) for 1 h. The pretreated cells were then co-incubated with RPDiD NPs for 0.5 h. The cells were then collected and washed by PBS three times for flow cytometry analysis.

2.11. Cytotoxicity and apoptosis of RPE NPs

WERI-Rb-1 cells were seeded in a 48-well plate at density of 1×10^4 cells per well (0.2 mL) and incubated for 24 h. The cells were then treated with RPE NPs or PPE NPs with etoposide concentrations at 0, 0.125, 0.25, 0.5, and 1 μM. After 24 h incubation, 20 μL CCK-8 kit solution was added into each well. After 4 h further incubation, the absorbance of each well at 450 nm was measured by a microplate reader (SpectraMax M4). The relative cell viability was calculated as follows:

$$\text{Cell viability}\ (\%) = \frac{\text{Abs.in treated group}}{\text{Abs.in control group}} \times 100\%$$

For apoptosis analysis, the cells were seeded using the same methods and treated with RPE NPs or PPE NPs with etoposide concentration at 2 μM. After 24 h incubation, the cells were stained with an Annexin V-FITC apoptosis detection kit according to the protocol. The stained cells were analyzed by flow cytometry.

2.12. Animal model construction

BALB/c nude mice (male, 4–6 weeks) were obtained from the Centre for Comparative Medicine Research (Li Ka Shing Faculty of Medicine, The University of Hong Kong). Animal study protocol was approved by the Committee on the Use of Live Animals in Teaching and Research (CULATR) at The University of Hong Kong (CULATR No. 23–315). Animals were maintained at the conventional experimental holding area of Dexter H.C. Man Building at the Centre for Comparative Medicine Research. An orthotopic retinoblastoma-bearing mouse model was constructed according to our previous study [20]. Briefly, 40 mg/kg pentobarbital sodium was intraperitoneally injected for anesthesia, and 0.4 % oxybuprocaine hydrochloride was applied on the right eye for ocular local anesthesia. And then 0.5 % tropicamide was applied to dilate the pupil. WERI-Rb-1-Luc-GFP cells were suspended in PBS at a density of 10^4 cells/μL. With a micro syringe (33G, Hamilton), 2 μL cell suspension was slowly injected into the bottom of the vitreous cavity of the eye. After removal of the micro syringe, 0.5 % chloramphenicol was topically applied. After 7 days, progress of the inoculated retinoblastoma was monitored by detection of its luminescence by in vivo imaging system (IVIS Lumina X5, Perkin-Elmer) with intraperitoneal injection of 150 mg/kg D-luciferin potassium salt.

2.13. Intraocular distribution and retention

For the intraocular distribution and retention study, BALB/c nude mice with orthotopic retinoblastoma were randomly divided into two groups according to treatments: PPDiR NPs and RPDiR NPs. DiR dye concentration was quantified by a microplate reader (SpectraMax M4, Fig. S1c). The DiR-loaded nanoparticle solution (2 μL) was slowly intravitreally injected. Fluorescence signals of DiR were detected by IVIS at 3, 6, 10, 24, and 48 h post-injection. The intraocular DiR radiant efficiency value at each timepoint was calibrated by subtracting the background value as:

$$Radiant\ efficiency_{calibrated} = Radiant\ efficiency_{tested} - Radiant\ efficiency_{blank}$$

where 'Radiant efficiency$_{blank}$' means the background value of the corresponding mouse without DiR injection. After 48 h, the mice were euthanized, and the tumor-inoculated eyes were harvested for cryosectioning. Stained with DAPI for 10 min, the cryosections of the eyes were observed under a confocal microscope (Zeiss LSM 980). The arithmetic mean fluorescence intensity of DiR dye was analyzed by ZEISS ZEN 3.10 software.

2.14. In vivo antitumor efficacy

For evaluation of in vivo antitumor efficacy, BALB/c nude mice bearing orthotopic retinoblastoma were randomly divided into four groups according to treatments: PBS, Free etoposide, PPE NPs, and RPE NPs. The drug solution (2 μL) was slowly intravitreally injected with dosage of etoposide at 0.0269 mg/kg. With intraperitoneal injection of 150 mg/kg D-luciferin potassium salt, progress of retinoblastoma was monitored by IVIS every other day within 11 days after drug administration. On the 11th day, the mice were euthanized, and their eyes and major organs were harvested for hematoxylin and eosin (H&E) staining.

2.15. Statistical analysis

GraphPad Prism 9.5.1 software (GraphPad Software, Inc) was used for statistical analysis. Experiments were conducted three times or more independently. Data were presented as the mean ± standard deviation (S.D.). Two-tailed unpaired Student's *t*-test and one-way ANOVA were used to determine the statistical significance of differences, with significance levels defined as $*p < 0.05$, $**p < 0.01$, $***p < 0.001$, and $****p < 0.0001$.

3. Results and discussion

3.1. Preparation and characterization of WERI-Rb-1 cell membrane-coated nanoparticles

As a well-recognized biocompatible and biodegradable polymer, PLGA has been extensively employed to fabricate nanocarrier for drug delivery [21]. Based on a previously reported single emulsion method, we encapsulated the small-molecule chemotherapy drug etoposide into PLGA nanocarriers to fabricate PLGA-etoposide nanoparticles (PE NPs)

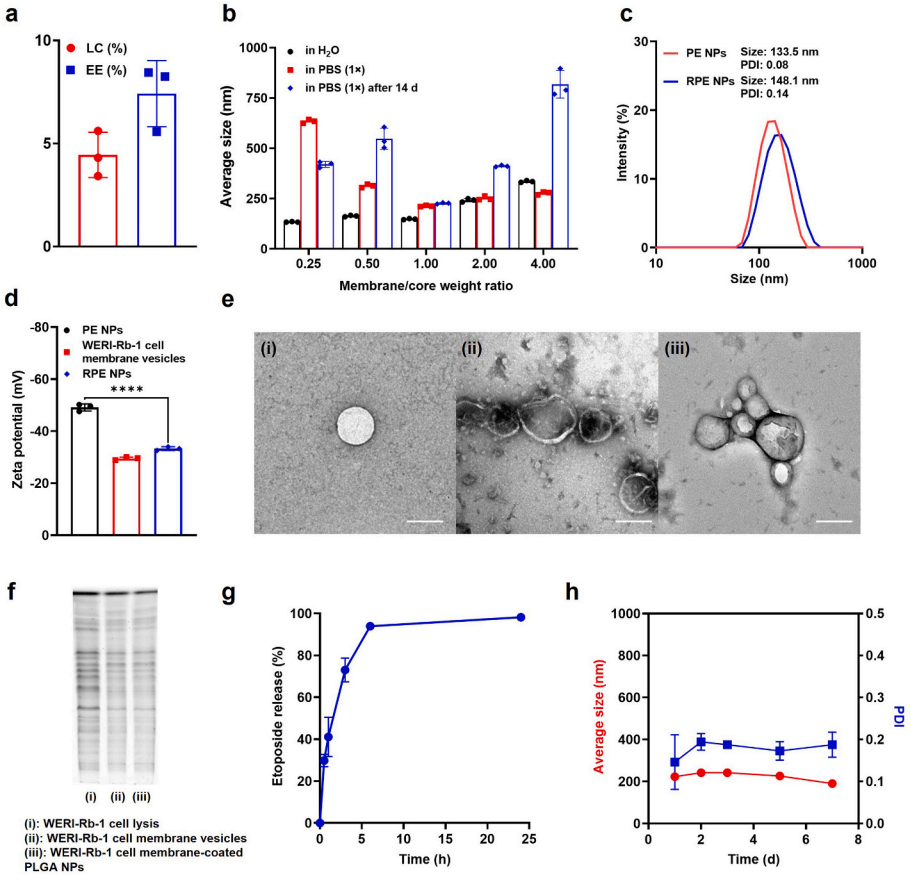

Fig. 1. Fabrication and characterization of RPE NPs. (a) Loading capacity (LC) and encapsulation efficiency (EE) of PE NPs ($n = 3$, mean ± SD). (b) Average size of RPE NPs at different membrane/core weight ratios in water, PBS, and PBS after 14 d ($n = 3$, mean ± SD). (c) Size distributions of PE NPs before and after WERI-Rb-1 cell membrane coating. (d) Zeta potential of PE NPs, WERI-Rb-1 membrane vesicles, and RPE NPs ($n = 3$, mean ± SD). $****p < 0.0001$, Student's *t-test*. (e) Transmission electron microscopy images of (i) PE NPs, (ii) WERI-Rb-1 cell membrane vesicles, and (iii) RPE NPs (Scale bar: 100 nm). (f) SDS-PAGE analysis result of (i) WERI-Rb-1 cell lysate, (ii) WERI-Rb-1 cell membrane vesicles, and (iii) WERI-Rb-1 cell membrane-coated PLGA nanoparticles. (g) Drug release profile of RPE NPs at 37 °C and 60 rpm ($n = 3$, mean ± SD). (h) Average sizes and PDIs of RPE NPs at room temperature in PBS over 7 days ($n = 3$, mean ± SD).

[19]. With high performance liquid chromatography (HPLC, Fig. S1a and Table S1), the loading capacity (LC) and encapsulation efficiency (EE) of etoposide were determined to be approximately 4.45 % and 7.42 %, respectively (Fig. 1a). The WERI-Rb-1 cell membrane was extracted through a series of procedures including cell harvest, cell lysis, and differential centrifugation purification. As a simple and efficient method, ultrasound water bath was adopted for WERI-Rb-1 cell membrane coating on PE NPs to obtain retinoblastoma cell membrane-coated PE NPs (RPE NPs). Compared with free etoposide, RPE NPs displayed the same UV–Visible absorption spectrum and a characteristic peak at 230 nm (Fig. S2), which also verifies the successful loading of etoposide. Due to charge screening effect induced by ions in the solution, bare or incompletely coated PLGA nanoparticles tend to aggregate in PBS [22]. Consequently, the mixing ratio of WERI-Rb-1 cell membrane versus PE NP cores (*w*/w) was optimized to screen out a relatively optimal coating formulation. As shown in Fig. 1b, when the membrane/core weight ratio equaled to 1:1, the particle size of RPE NPs displayed very slight increase in PBS after 14 d compared to the change at other ratios. As a result, 1:1 was selected as membrane/core weight ratio for RPE NPs preparation in the following experiments. As shown in Fig. 1c, with dynamic light scattering (DLS) testing, the average size of PE NPs was measured to increase from around 133.5 nm to around 148.1 nm after coating in deionized water. The polydispersity indexes (PDIs) of the nanoparticles were both below 0.2 before and after coating, which confirmed a narrow size distribution. The zeta potential of RPE NPs was also measured by DLS. As shown in Fig. 1d, coating with WERI-Rb-1 cell membrane, the zeta potential of PE NPs significantly increased from around −49.1 mV to −33.3 mV, which was similar to that of WERI-Rb-1 cell membrane vesicles (−29.5 mV). The similarity indicated the success of coating. The morphology of RPE NPs was imaged by a transmission electronic microscope (TEM). As presented in Fig. 1e, compared to bare spherical PE NPs (i) and hollow WERI-Rb-1 cell membrane vesicles (ii), RPE NPs displayed a clear core-shell structure (iii), which proved the successful coating. With cancer cell membrane coating, various functional proteins on the surface of the cell membrane could be concomitantly modified on core nanoparticles. Among them, proteins responsible for intercellular binding are essential for the reported homotypic targeting effect [23]. Hence, we presented protein profile of RPE NPs through SDS-PAGE. As presented in Fig. 1f, plasma membrane proteins were well preserved throughout the membrane extraction and coating process, verifying the functionalization of PE NPs by WERI-Rb-1 cell membrane coating.

To evaluate the drug release profile, paralleling groups of RPE NPs were loaded in dialysis devices in PBS at 37 °C under gentle shaking. The RPE NPs were retrieved at different timepoints to quantify the remaining amount of encapsulated etoposide. As shown in Fig. 1g, RPE NPs presented a burst release of etoposide (around 73 %) within the first 3 h, followed by a sustained release. As an essential property for application and translation, the colloidal stability of RPE NPs was evaluated by continuous monitoring of their average sizes and PDIs in PBS at room temperature. As shown in Fig. 1h, during 7 days post-fabrication, the average sizes of RPE NPs were around 200 nm while the PDIs remained to be around 0.2, showing good stability.

3.2. *In vitro activity of WERI-Rb-1 cell membrane-coated nanoparticles*

The homotypic targeting effect has been widely reported for many types of cancer cell membrane-coated nanoparticles. Herein, we verified the targeting effect through cellular uptake test. First, the lipophilic fluorescent dye 1,1'-dioctadecyl-3,3,3′,3'-tetramethylindodicarbocyanine,4-chlorobenzenesulfonate salt (DiD, ex/em = 644/663 nm) was loaded in PLGA nanoparticles to fabricate retinoblastoma cell membrane-coated PLGA-DiD nanoparticles (RPDiD NPs). There were two types of functionalized PLGA-DiD NPs set as control groups. As PEGylation is a widely adopted modification method to improve nanoparticles stability, circulation time, and tumor accumulation, mPEG-PLGA-DiD nanoparticles (PPDiD NPs, Fig. S3a and b) was set as a control group [24]. The other one was cyclic RGD-PEG-PLGA-DiD nanoparticles (cRGD-PPDiD NPs, Fig. S4a and b) as cyclic RGD (cRGD) peptide is a targeting ligand to integrin $\alpha_v\beta_3$ overexpressed on tumor cells [25]. WERI-Rb-1 cells were incubated with DiD-loaded nanoparticles for 0.5 h and then washed before flow cytometry analysis. As shown in Fig. 2a and b, cRGD-PPDiD NPs exhibited significantly higher uptake by WERI-Rb-1 cells compared to PPDiD NPs, attributed to the targeting effect of cRGD peptide. Nevertheless, RPDiD NPs presented significantly higher cellular uptake compared to both control groups, indicating excellent targeting effect. Confocal laser scanning microscopy (CLSM) was utilized to assess the colocalization of the nanoparticles with WERI-Rb-1 cells. As displayed in Fig. 2c, WERI-Rb-1 cells incubated with RPDiD NPs presented the strongest far-red signal of DiD dye, consistent with the flow cytometry results. The homotypic targeting effect of RPDiD NPs was further verified by flow cytometry. RPDiD NPs were incubated with WERI-Rb-1 cells, 4T1 mouse breast cancer cells, and KYSE450 human esophageal cancer cells for 0.5 h, respectively. The cells were washed by PBS and analyzed by flow cytometry for uptake level testing. As shown in Fig. 2d, RPDiD NPs had the highest uptake by WERI-Rb-1 cells among all tested cell types, demonstrating the homotypic property.

We continued to explore the endocytosis mechanism of the WERI-Rb-1 cell membrane-coated nanoparticles. WERI-Rb-1 cells were pretreated with different endocytosis pathway inhibitors, including mβ-CD (a lipid rafts-mediated endocytosis inhibitor), CPZ (a clathrin-mediated endocytosis inhibitor), EIPA (a macropinocytosis inhibitor), and genistein (a caveolae-mediated endocytosis inhibitor). The pretreated WERI-Rb-1 cells were then incubated with RPDiD NPs for 0.5 h. As shown in Fig. 2e, the flow cytometry results for cellular uptake showed that only CPZ displayed significant inhibition on the uptake of RPDiD NPs, illustrating that the endocytosis of the WERI-Rb-1 cell membrane-coated nanoparticles was mainly mediated by a clathrin-dependent pathway. Next, we measured the cytotoxicity of RPE NPs through cell counting kit-8 (CCK-8) assay. WERI-Rb-1 cells were incubated with mPEG-PLGA-etoposide (PPE NPs) and RPE NPs at increasing etoposide concentrations. As shown in Fig. 2f, RPE NPs presented significant cytotoxicity enhancement against WERI-Rb-1 cells compared with PPE NPs at etoposide concentration of 0.5 μM and above. Apoptosis profiles of WERI-Rb-1 cells treated with PPE NPs and RPE NPs were presented in Fig. 2g and h. As shown, the WERI-Rb-1 cells treated with RPE NPs presented lower rates of late apoptosis (Q2) but higher rates of total apoptosis (Q2 + Q4), which was consistent with the enhanced cytotoxicity.

3.3. *Intraocular retention and targeting of WERI-Rb-1 cell membrane-coated nanoparticles*

Encouraged by the homotypic targeting effect and excellent cytotoxicity in vitro, we further evaluated the performance of the WERI-Rb-1 cell membrane-coated nanoparticles in an orthotopic retinoblastoma-bearing mouse model. The model was established by intravitreal injection of WERI-Rb-1-Luc-GFP cells into subretinal space of the right eye of BALB/c nude mice. As shown in Fig. 3a, the mouse successfully inoculated with retinoblastoma exhibited obvious leukocoria, which is a typical clinical symptom of retinoblastoma. Currently, there has been plenty of imaging molecules developed for in vivo nanoparticles tracing and cancer treatments [26,27]. Herein, to evaluate intraocular retention, near-infrared lipophilic dye 1,1′-dioctadecyl-3,3,3′,3′-tetramethylindotricarbocyanine iodide (DiR, ex/em = 748/780 nm) was loaded to obtain WERI-Rb-1 cell membrane-coated DiR-loaded PLGA nanoparticles (RPDiR NPs). After intravitreal injection, the radiant efficiency of the DiR dye was measured by in vivo imaging system (IVIS) and calibrated by subtracting background values (Fig. S5). As shown in Fig. 3b and c, RPDiR NPs had presented significantly higher retention than mPEG-PLGA-DiR nanoparticles (PPDiR NPs) since 4 h after injection. To further evaluate the intraocular targeting capability of the

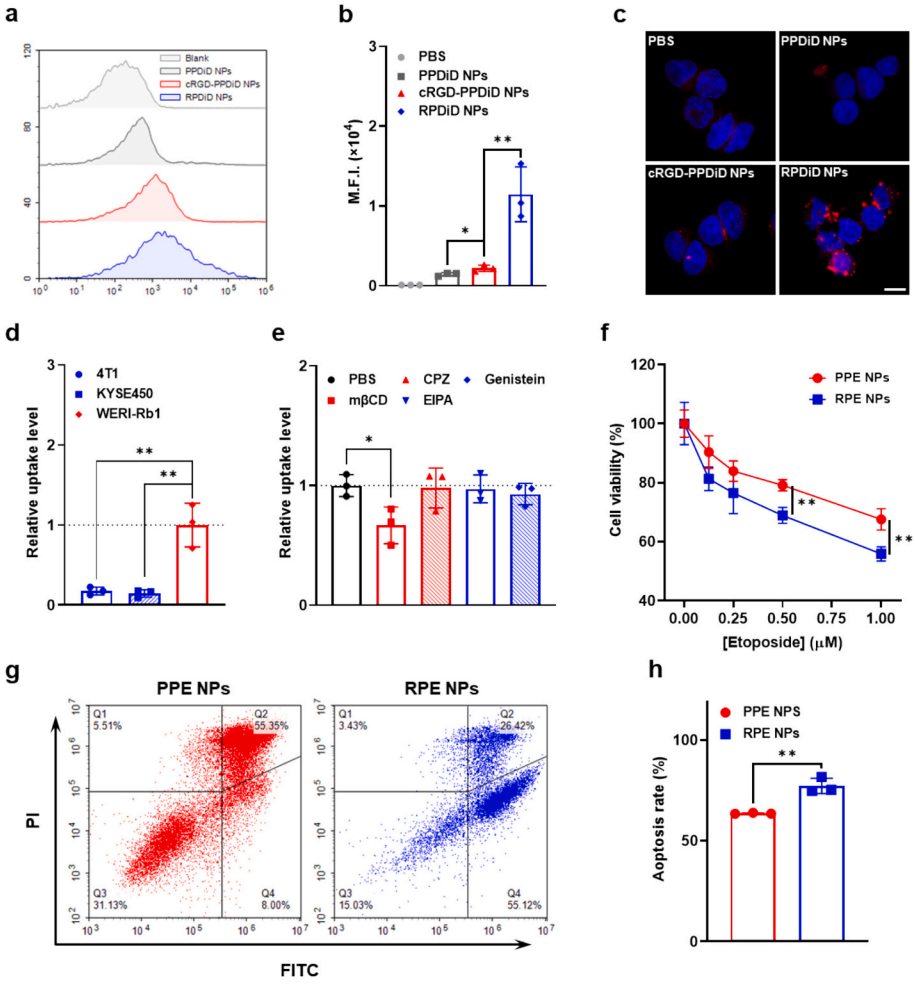

Fig. 2. In vitro activity of WERI-Rb-1 cell membrane-coated nanoparticles. (a) Representative flow cytometry results of WERI-Rb-1 cells' uptake of DiD after different treatments and (b) corresponding quantification analysis ($n = 3$, mean ± SD). *$p < 0.05$, **$p < 0.01$, Student's *t-test*. (c) CLSM images of WERI-Rb-1 cells after different treatments. (Blue: Hoechst blue 33342, far red: DiD, scale bar: 20 μm). (d) Relative uptake level of RPDiD NPs by different types of cancer cells ($n = 3$, mean ± SD). **$p < 0.01$, Student's *t-test*. (e) WERI-Rb-1 cells' uptake of RPDiD NPs after pretreatments with different endocytosis pathway inhibitors (n = 3, mean ± SD). *$p < 0.05$, Student's *t-test*. (f) WERI-Rb-1 cells' viability after different treatments (n = 3, mean ± SD). **$p < 0.01$, Student's *t-test*. (g) Representative flow cytometry results of WERI-Rb-1 cells' apoptosis profile after different treatments and (h) corresponding quantification analysis (n = 3, mean ± SD). **$p < 0.01$, Student's *t-test*. (For interpretation of the references to colour in this figure legend, the reader is referred to the web version of this article.)

nanoparticles, the mice were euthanized 48 h post-injection. The retinoblastoma-bearing eyes were harvested for cryosectioning. As shown in Fig. 3d and e, in the retinoblastoma region where the green fluorescent protein (GFP) was significantly expressed (marked by white dash lines), the RPDiR NPs group showed significantly higher DiR accumulation than the PPDiR NPs group. Taken together, these results revealed the superior retinoblastoma-targeting capability of RPDiR NPs.

3.4. In vivo antitumor efficacy of WERI-Rb-1 cell membrane-coated nanoparticles

The therapeutic efficacy of RPE NPs was then evaluated in the same murine model. The scheme of the experiments was presented in Fig. 4a. After a single-dose intravitreal injection of the drug solutions, the progression of retinoblastoma was monitored by IVIS every other day. As shown in Fig. 4b, compared to other treatments, including PBS, free etoposide, and PPE NPs, RPE NPs exhibited significantly greater inhibition of retinoblastoma progression, suggesting excellent antitumor efficacy. As shown in Fig. 4c, during the monitoring period, the body weight of all the mice remained stable, indicating biosafety of RPE NPs. For IVIS imaging, D-luciferin potassium salt solution was intraperitoneally injected as a substrate of luciferase expressed in retinoblastoma. Representative luminescence images of the retinoblastomas in all groups during the monitoring period are displayed in Fig. 4d. It can be observed that the mouse treated with RPE NPs showed significant inhibition of retinoblastoma progression, whereas the other three control groups presented substantial tumor growth. As a hallmark of retinoblastoma, leukocoria of the mice after different treatments were imaged by the Micron IV system. Representative images are presented in Fig. 4e. As shown, the mice injected with PBS and free etoposide both still showed significant leukocoria, indicating progression of retinoblastoma. In contrast, leukocoria in the eye treated with PPE NPs appeared to be significantly reduced, suggesting a moderate inhibitory effect on tumor growth. Notably, leukocoria disappeared in the eye treated with RPE NPs at the same dosage. Inhibition of retinoblastoma was further confirmed by analyzing the eyeball sections stained with hematoxylin

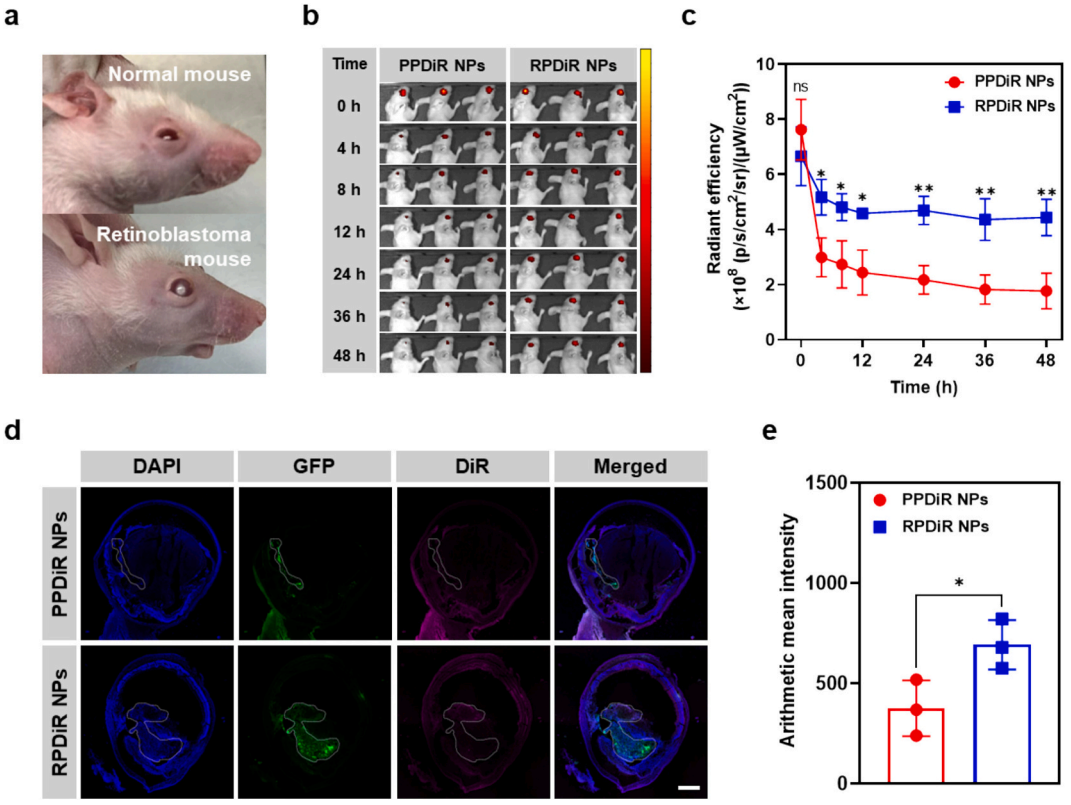

Fig. 3. Intraocular targeting of RPDiR NPs. (a) Photographs of a normal mouse eye and a retinoblastoma-bearing mouse eye. (b) Representative IVIS images showing DiR fluorescence retention in the eyes of retinoblastoma-bearing mice. (c) Quantification analysis of DiR fluorescence intensity in panel (b) ($n = 3$, mean ± SD). *$p < 0.05$, **$p < 0.01$, Student's *t*-test (comparison between the 'PPDiR NPs' group and the 'RPDiR NPs' group at each timepoint). (d) Representative cryosections of intravitreally injected mouse eyes (Blue: DAPI; green: green fluorescent protein expressed by WERI-Rb-1-Luc-GFP; far red: DiR. Scale bar: 500 μm). (e) Quantification analysis of the arithmetic mean intensity of DiR in the retinoblastoma area of each harvested eye (n = 3, mean ± SD). *$p < 0.05$, Student's t-test. (For interpretation of the references to colour in this figure legend, the reader is referred to the web version of this article.)

and eosin (H&E). As shown in Fig. 4f, the eyes injected with PBS, free etoposide, or PPE NPs presented prominent area of retinoblastoma. However, the eye injected with RPE NPs at the same dosage showed an intact and healthy retinal structure, indicating elimination of retinoblastoma and excellent retinal biosafety. Major organs of the mice after different treatments were also collected for sections and H&E staining (Fig. S6). All the organs displayed normal physiological morphologies, indicating systemic biosafety. Overall, the results of in vivo studies confirmed the targeted delivery and notable antitumor efficacy of WERI-Rb-1 cell membrane-coated nanoparticles against retinoblastoma.

4. Conclusion and discussion

In summary, we fabricated WERI-Rb-1 cell membrane-coated PLGA nanoparticles for the treatment of retinoblastoma through a single-dose intravitreal injection. Based on homotypic targeting effect, the nanoparticles showed significant targeting ability to WERI-Rb-1 cells. Loaded with the FDA-approved chemotherapeutic drug etoposide, RPE NPs presented excellent biosafety and superior antitumor efficacy in an orthotopic retinoblastoma-bearing mouse model. To our knowledge, it is the first application of cancer cell membrane-coated nanoparticles for intraocular tumor treatment. Combined with intravitreal injection, a local administration method, high drug delivery efficiency was achieved. Furthermore, this localized and targeted delivery requires a low dosage and reduced administration frequency, which minimizes side effects such as unwanted systemic toxicity [28]. In addition to retinoblastoma, the cancer cell membrane-coated nanoplatform may also be applied for targeted drug delivery in the treatment of other intraocular tumors such as choroidal melanoma.

Although single-dose injection has been proven to be effective for tumor inhibition, damage to intraocular structures may result in endophthalmitis and more severe consequences if not operating properly [29]. Future studies may focus on the development of alternative dosage forms such as eyedrops. Meanwhile, other tools such as injectable hydrogels can also be employed to elongate the nanoparticles retention for efficacy improvement. The simple design and fabrication process of the WERI-Rb-1 cell membrane-coated nanoplatform show great potential for clinical translation. However, some issues remain to be addressed, such as immunocompatibility. Potential solutions include designing a universal cell line with immunogenicity-related genes genetically knocked out [30]. Above all, WERI-Rb-1 cell membrane-coated nanoparticles offer a novel, efficient, and safe strategy for intraocular tumor therapy. The study also advances the development of biomimetic drug delivery systems for the treatment of intraocular diseases.

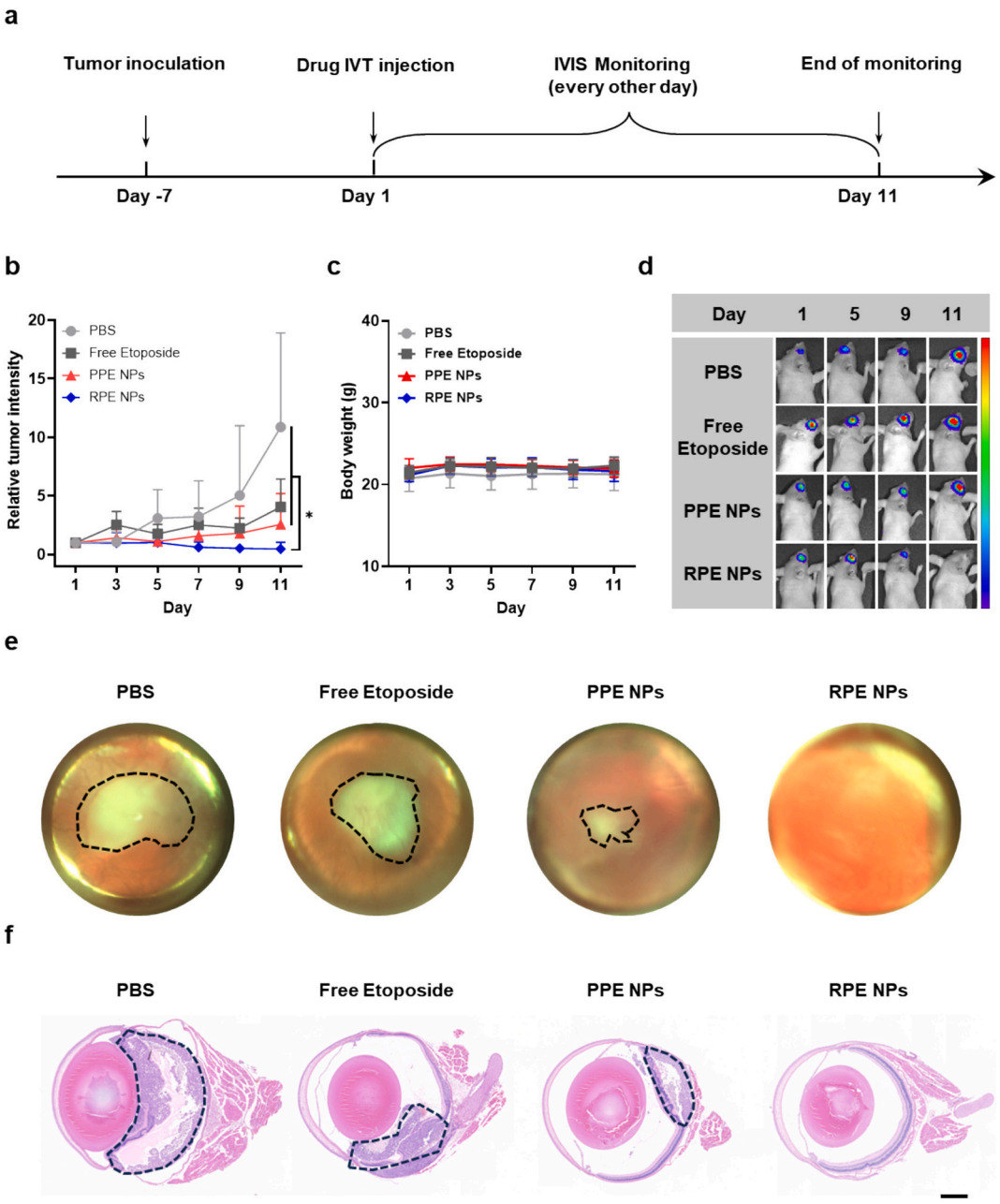

Fig. 4. In vivo antitumor efficacy of RPE NPs. (a) Scheme of in vivo antitumor efficacy evaluation experiments. IVT: intravitreal. (b) Tumor progression profile during the monitoring period ($n = 4$, mean ± SD). *$p < 0.05$, one-way ANOVA. (c) Average body weight change curves of the mice with different treatments (n = 4). (d) Representative bioluminescence images of the retinoblastomas in the mice subjected to different treatments during the monitoring period. (e) Representative photographs of the eyes from the mice subjected to different treatments at the end of the monitoring period. (f) Representative H&E-stained eyeball histology sections of the eyeball from the mice subjected to different treatments at the end of the monitoring period (scale bar: 500 μm).

Acknowledgements and funding sources

We acknowledge the assistance of the Faculty Core Facility of Li Ka Shing Faculty of Medicine, The University of Hong Kong. We thank YouTube Channel 'PowerPoint University' for providing the graphical template of the eye structure. This work was supported by the Seed Fund for Basic Research of The University of Hong Kong (No. 2202100724).

CRediT authorship contribution statement

Yichi Zhang: Writing – review & editing, Writing – original draft, Visualization, Validation, Software, Resources, Methodology, Investigation, Formal analysis, Data curation, Conceptualization. **Kaiqi Long:** Writing – review & editing, Methodology, Investigation, Data curation, Conceptualization. **Ka Yi Lee:** Writing – review & editing, Methodology, Investigation, Data curation. **Jia Li:** Writing – review & editing, Investigation, Data curation. **Shuting Xu:** Writing – review & editing, Investigation, Data curation. **Kang Chen:** Writing – review & editing, Investigation, Data curation. **Xi Chen:** Writing – review & editing, Investigation, Data curation. **Qingyi Dai:** Writing – review & editing, Investigation, Data curation. **Yifan Lin:** Writing – review & editing, Formal analysis. **Changyou Zhan:** Writing – review & editing, Formal analysis. **Weiping Wang:** Writing – review & editing, Supervision, Resources, Project administration, Methodology, Investigation, Funding acquisition, Formal analysis, Data curation, Conceptualization.

Declaration of competing interest

W.W. and Y.Z. are inventors of a US patent application (No. 18/889,021), submitted by The University of Hong Kong, which covers the preparation method of the WERI-Rb-1 cell membrane-coated nanoparticles in this study and their in vivo applications. All other authors declare no competing interests.

Appendix A. Supplementary data

Supplementary data to this article can be found online at https://doi.org/10.1016/j.jconrel.2025.113939.

Data availability

Data will be made available on request.

References

[1] I. Aerts, L. Lumbroso-Le Rouic, M. Gauthier-Villars, H. Brisse, F. Doz, L. Desjardins, Retinoblastoma, Orphanet J. Rare Dis. 1 (2006) 31.
[2] H. Dimaras, K. Kimani, E.A.O. Dimba, P. Gronsdahl, A. White, H.S.L. Chan, B. L. Gallie, Retinoblastoma, Lancet 379 (2012) 1436–1446.
[3] R. Leclerc, J. Olin, An overview of retinoblastoma and enucleation in pediatric patients, AORN J. 111 (2020) 69–79.
[4] A.E. Rizzuti, I.J. Dunkel, D.H. Abramson, The adverse events of chemotherapy for retinoblastoma: what are they? Do we know? Arch. Ophthalmol. 126 (2008) 862–865.
[5] A. Velentza-Almpani, N. Ibeanu, T. Liu, C. Redhead, P. Tee Khaw, S. Brocchini, S. Awwad, Y. Bouremel, Effects of flow hydrodynamics and eye movements on intraocular drug clearance, Pharmaceutics 14 (2022) 1267.
[6] I. Brigger, C. Dubernet, P. Couvreur, Nanoparticles in cancer therapy and diagnosis, Adv. Drug Deliv. Rev. 64 (2012) 24–36.
[7] M. Wang, M. Thanou, Targeting nanoparticles to cancer, Pharmacol. Res. 62 (2010) 90–99.
[8] H. Wang, Y. Liu, R. He, D. Xu, J. Zang, N. Weeranoppanant, H. Dong, Y. Li, Cell membrane biomimetic nanoparticles for inflammation and cancer targeting in drug delivery, Biomater. Sci. 8 (2020) 552–568.
[9] M. Li, Z. Xu, L. Zhang, M. Cui, M. Zhu, Y. Guo, R. Sun, J. Han, E. Song, Y. He, Y. Su, Targeted noninvasive treatment of choroidal neovascularization by hybrid cell-membrane-cloaked biomimetic nanoparticles, ACS Nano 15 (2021) 9808–9819.
[10] W. Xia, C. Li, Q. Chen, J. Huang, Z. Zhao, P. Liu, K. Xu, L. Li, F. Hu, S. Zhang, T. Sun, C. Jiang, C. Zhao, Intravenous route to choroidal neovascularization by macrophage-disguised nanocarriers for mTOR modulation, Acta Pharm. Sin. B 12 (2022) 2506–2521.
[11] J. Ding, J. Lu, Q. Zhang, Y. Xu, B. Song, Y. Wu, H. Shi, B. Chu, H. Wang, Y. He, Camouflage nanoparticles enable in situ bioluminescence-driven optogenetic therapy of retinoblastoma, ACS Nano 17 (2023) 7750–7764.
[12] J.C. Harris, M.A. Scully, E.S. Day, Cancer cell membrane-coated nanoparticles for cancer management, Cancers 11 (2019) 1836.
[13] X. Liu, Y. Sun, S. Xu, X. Gao, F. Kong, K. Xu, B. Tang, Homotypic cell membrane-cloaked biomimetic nanocarrier for the targeted chemotherapy of hepatocellular carcinoma, Theranostics 9 (2019) 5828–5838.
[14] S.-Y. Li, H. Cheng, W.-X. Qiu, L. Zhang, S.-S. Wan, J.-Y. Zeng, X.-Z. Zhang, Cancer cell membrane-coated biomimetic platform for tumor targeted photodynamic therapy and hypoxia-amplified bioreductive therapy, Biomaterials 142 (2017) 149–161.
[15] L. Rao, G.-T. Yu, Q.-F. Meng, L.-L. Bu, R. Tian, L.-S. Lin, H. Deng, W. Yang, M. Zan, J. Ding, A. Li, H. Xiao, Z.-J. Sun, W. Liu, X. Chen, Cancer cell membrane-coated nanoparticles for personalized therapy in patient-derived xenograft models, Adv. Funct. Mater. 29 (2019) 1905671.
[16] M. Ashrafizadeh, A. Zarrabi, A. Bigham, A. Taheriazam, Y. Saghari, S. Mirzaei, M. Hashemi, K. Hushmandi, H. Karimi-Maleh, E. Nazarzadeh Zare, E. Sharifi, Y. N. Ertas, N. Rabiee, G. Sethi, M. Shen, (Nano)platforms in breast cancer therapy: drug/gene delivery, advanced nanocarriers and immunotherapy, Med. Res. Rev. 43 (2023) 2115–2176.
[17] R.C. McFall, T.W. Sery, M. Makadon, Characterization of a new continuous cell line derived from a human retinoblastoma1, Cancer Res. 37 (1977) 1003–1010.
[18] A. Montecucco, F. Zanetta, G. Biamonti, Molecular mechanisms of etoposide, EXCLI J. 14 (2015) 95.
[19] J.H. Park, Y. Jiang, J. Zhou, H. Gong, A. Mohapatra, J. Heo, W. Gao, R.H. Fang, L. Zhang, Genetically engineered cell membrane–coated nanoparticles for targeted delivery of dexamethasone to inflamed lungs, Sci. Adv. 7 (2021) eabf7820.
[20] K. Long, Y. Yang, W. Lv, K. Jiang, Y. Li, A.C.Y. Lo, W.C. Lam, C. Zhan, W. Wang, Green light-triggered intraocular drug release for intravenous chemotherapy of retinoblastoma, Adv. Sci. 8 (2021) 2101754.
[21] F. Danhier, E. Ansorena, J.M. Silva, R. Coco, A. Le Breton, V. Préat, PLGA-based nanoparticles: an overview of biomedical applications, J. Control. Release 161 (2012) 505–522.
[22] Y. Jiang, N. Krishnan, J. Zhou, S. Chekuri, X. Wei, A.V. Kroll, C.L. Yu, Y. Duan, W. Gao, R.H. Fang, L. Zhang, Engineered cell-membrane-coated nanoparticles directly present tumor antigens to promote anticancer immunity, Adv. Mater. 32 (2020) 2001808.
[23] R.H. Fang, C.-M.J. Hu, B.T. Luk, W. Gao, J.A. Copp, Y. Tai, D.E. O'Connor, L. Zhang, Cancer cell membrane-coated nanoparticles for anticancer vaccination and drug delivery, Nano Lett. 14 (2014) 2181–2188.
[24] J.V. Jokerst, T. Lobovkina, R.N. Zare, S.S. Gambhir, Nanoparticle PEGylation for imaging and therapy, Nanomedicine 6 (2011) 715–728.
[25] S. Zitzmann, V. Ehemann, M. Schwab, Arginine-glycine-aspartic acid (RGD)-peptide binds to both tumor and tumor-endothelial cells in vivo, Cancer Res. 62 (2002) 5139–5143.
[26] H. Li, Y. Kim, H. Jung, J.Y. Hyun, I. Shin, Near-infrared (NIR) fluorescence-emitting small organic molecules for cancer imaging and therapy, Chem. Soc. Rev. 51 (2022) 8957–9008.
[27] S. Roy, N. Bag, S. Bardhan, I. Hasan, B. Guo, Recent progress in NIR-II fluorescence imaging-guided drug delivery for cancer theranostics, Adv. Drug Deliv. Rev. 197 (2023) 114821.
[28] O.M. Kutova, E.L. Guryev, E.A. Sokolova, R. Alzeibak, I.V. Balalaeva, Targeted delivery to tumors: multidirectional strategies to improve treatment efficiency, Cancers 11 (2019) 68.
[29] A.P. Hunyor, R. Merani, A. Darbar, J.-F. Korobelnik, P. Lanzetta, A.A. Okada, Topical antibiotics and intravitreal injections, Acta Ophthalmol. 96 (2018) 435–441.
[30] R.H. Fang, W. Gao, L. Zhang, Targeting drugs to tumours using cell membrane-coated nanoparticles, Nat. Rev. Clin. Oncol. 20 (2023) 33–48.